

University of Waterloo
Faculty of Engineering
Electrical & Computer Engineering

Atomic Layer Epitaxy: A Review

Prepared by

Han Liu

Table of Contents

List of Figures	3
List of Tables	4
1.0 Introduction	5
2.0 History	5
3.0 Theory	7
4.0 Processes	11
4.1 Substrate Preparation	11
4.2 Solid Phase Epitaxy	12
4.3 Liquid Phase Epitaxy	14
4.4 Vapor Phase Epitaxy	15
4.5 Molecular Beam Epitaxy	18
4.6 Electrochemical Epitaxy	20
5.0 Applications	22
5.1 Quantum Structures & Superlattices	25
6.0 Summary	27
Glossary	28
Reference	29

List of Figures

Figure 1. ALE process for atomic monolayer deposition	4
Figure 2. Dependence of the critical thickness for 2D-to-3D transition	10
Figure 3. Molecular dynamic simulation of Si SPE at 1800 K	13
Figure 4. Layer-by-layer preparation of SCP systems	15
Figure 5. A silicon VPE barrel reactor	16
Figure 6. Schematic and photograph of a typical MBE system.....	20
Figure 7. Two common ECALE systems: (a) thin layer flow cell (b) H cell	22
Figure 8. ALD controlled nano-porous alumina membrane.....	25
Figure 9. Growth sequence of $\text{GaAs}_{0.8}\text{P}_{0.2}$ via ALE	26

List of Tables

Table 1. The characteristic features of ALE	4
Table 2. Performance comparison of ALE & sputtered buffer layers	23
Table 3. ALE in solar cell applications	23

ATOMIC LAYER EPITAXY

1.0 Introduction

This review outlines recent development in the field of atomic layer epitaxy (ALE) since its first demonstration by Tuomo Suntola in 1974 [1], with a focus on its numerous applications in technologies such as transistors, optics, displays, solar cells and medical devices. The first section aims to provide a comprehensive overview of the subject. The review begins with the history of ALE to provide information regarding the motivation behind its invention followed by a brief description of its working principle. The report then delves into two mathematical models that describe the physical reality of ALE processes. The first Langmuir adsorption isotherm differential equation-based model aims to predict film thickness per deposition cycle and the second Frenkel-Kontorova energy minimization principle based model aims to predict morphology of the thin film. Equipped with a deeper understanding of the underlying mechanisms in ALE, the third section concentrates on various processes, examining members within the ALE family including solid phase epitaxy, liquid phase epitaxy, vapor phase epitaxy and electrochemical epitaxy. The molecular beam epitaxy, a member within the vapor phase epitaxy group that has recently received great research interest, is covered in more detail. The final section places its emphasis on applications of ALE. Besides the devices mentioned above, research topics in ALE nanostructures are covered including superlattices, quantum wires and quantum dots. The review follows a modular approach. The introduction, theory, process and application sections are self-contained enough so that readers may start at any part of this review without feeling overwhelmed.

2.0 History

Atomic layer epitaxy (ALE) refers the thin film growth technique based on the repetition of self-limiting solid-solid, liquid-solid and gas-solid reactions under saturated conditions by supplying complementary elements of the intended compound to a substrate surface in a cyclic manner [1]. “Epi-taxy”, meaning “on-arrangement” in Greek, was coined by its inventor Tuomo Suntola to emphasize the surface control feature of the process, thus differentiating it from the traditional source-controlled deposition methods such as evaporation and sputtering [1]. The invention of ALE was motivated by the need to replace the high-vacuum equipment with more compact flow-type reactors for the reliable fabrication

electroluminescent display panels (EDP) [1]. The first ALE-made light-emitting ZnS layer was grown in 1974 and X-ray diffraction (XRD) revealed the hexagonal crystalline structure of the thin film, compared to the cubic crystalline structure commonly observed using conventional techniques [1]. This structural difference manifested itself as the bright yellow instead of the dark orange color seen in EDPs at the time [1]. In spite of being initially conceived for EDPs, the application of ALE is far-reaching, and the technique have been implemented in most semiconductor devices. Comparing to traditional techniques, the main advantage of ALE lies in its capability of consistently producing uniform conformal thin films with high homogeneity and free of pinholes [2]. Based on the characteristic features of ALE and their inherent implications for film deposition as a consequence, a comprehensive list of its practical advantages has been tabulated by Ritala et al., shown in Table 1 [3].

Epitaxy can be roughly categorized into two group, homoepitaxial growth where the chemical composition of substrate and deposit is identical and heteroepitaxial growth where they are different. Royer, who coined the term “epitaxy”, demonstrated through X-ray diffraction that oriented growth is more probable when the coincident factor, calculated from the lattice constants of substrate and film, is low [4]. Technically, as the deposited film becomes thicker, the heteroepitaxial process may be approximated as homoepitaxial due to growingly negligible strain, under the condition that the film layer does not exceed critical thickness where interfacial misfit dislocations occur [4]. As stated previously, one of the greatest appeals of ALE is its capability of uniform monolayer deposition, which is only feasible when adatom descension from nucleation islands is energetically favorable [5]. Physically, this means epitaxy processes need to create a condition where the barrier of downward motion is lower than the diffusion activation energy at step edges [5]. With this goal in mind, the natural pursue is to either decrease the edge barrier so that it becomes statistically more probable to surmount it or to increase the adatom mobility so that the visiting frequency is enhanced [5]. In practice, this is achieved by adjusting the growth parameters and Rosenfeld et al. have demonstrated the effects of substrate temperature, deposition rate, ion beam and surfactant incorporation in their comprehensive review. The next section of this review will focus on the theoretical aspects of ALE [5].

Table 1. The characteristic features of ALE [3]

Characteristic Features of ALE	Inherent Implications for Film Deposition	Practical Advantages
Self-limiting growth process	<ul style="list-style-type: none"> • Cycle-dependent film thickness • No need for reactant flux homogeneity • Atomic control over material composition 	<ul style="list-style-type: none"> • Accurate & simple thickness control • Large-area & large-batch capability • Excellent conformality & reproducibility • Straightforward scale-up • Unaffected by inconstant precursors vaporization rates
Separate dosing of reactants	<ul style="list-style-type: none"> • No gas phase reaction 	<ul style="list-style-type: none"> • Effective material utilization
Wide processing temperature windows	<ul style="list-style-type: none"> • Sufficient time for each reaction step • Readily matched processing condition for each material 	<ul style="list-style-type: none"> • High-quality products at low processing temperatures • Continuous multilayer process capability

3.0 Theory

Generally, ALE is performed by sequentially feeding elemental reactants of the compound of interest to the wafer surface and one full or partial monolayer is grown at each step through additive chemisorption. Alternatively, it is also possible to supply compound reactants and condition exchange reaction between the exterior and bulk phases. Essentially, if the bond strength between surface and adatoms is sufficiently great and the substrate temperature is high enough to evaporate any subsequent adlayer, then only the first chemisorbed monolayer may remain attached [6]. With each exposure cycle, the film grows thicker, thus ALE can be considered a quasi-digital process [6]. It is imperative to ensure compound stability under the processing temperature or its decomposition will become a source of impurity within the thin film [2]. In either case, the common characteristic is the surface saturation at each reaction step which leads to incremental uniform growth. In other words, the deposition thickness depends solely on the saturation density [2]. Figure 1 obtained from its inventor Tuomo Suntola's review paper in 1992 illustrates the ideal ALE process with one monolayer per deposition cycle [2].

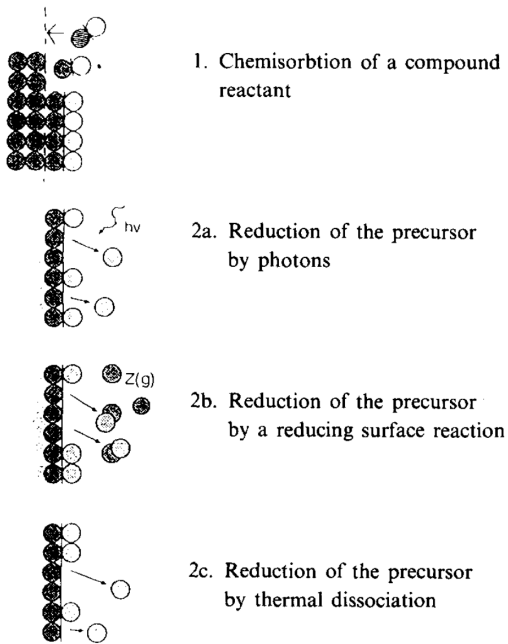


Figure 1. ALE process for atomic monolayer deposition [2].

For a simple vapor phase epitaxy $B(s) + A(g) = BA(s)$, the surface occupation may be modelled by Equation 1 under the assumption of low re-evaporation [7]. $N_0(A)$ is the saturation density of A atoms on a surface B at a specific process temperature and exposure time [7]. $t(A)$ is the exposure time of $A(g)$, $t_0(A)$ is the quotient of $N_0(A)$ and hitting rate H_A [7]. It is evident that as H_A increases, $t_0(A)$ decreases and the exponential term reaches 0 faster [7]. This means the surface occupation approaches the limit set forth by $N_0(A)$ faster [7]. Specifically, in an open system, the hitting rate $H_A(\text{open})$ is a function of the flux of A and the system's geometry factor [7]. On the other hand, in a closed system, the hitting rate $H_A(\text{closed})$ is a function of the partial pressure of A , its atomic mass and the process temperature [7]. Further, $N_0(A)$ refers to the product of surface coverage $f_s(A_B)$ and the maximum allowable surface density $N_s(A)$ given the lattice direction of $B(s)$ [7]. It self-evident that $N_s(A)$ represents the ideal “one full monolayer per cycle” occupation [7]. It is worth pointing out that the Langmuir model assumption that the adsorption of one atom or molecule is not influenced by the presence of other already adsorbed atoms or molecules does not hold true in real life scenarios [7].

$$[A(s)] = N_0(A)(1 - e^{-t(A)/t_0(A)}) \quad (\text{Equation 1})$$

In reality, due to insufficient reactant dosage, intermittent purging induced re-evaporation or bulky molecule steric hinderance, the ALE process commonly operates in the inherent non-ideal mode. During the non-overlapping alternate injection of reactants, incomplete coverage exchange between the preceding and subsequent elements occurs inevitably. To translate the microscopic processes into macroscopic predictions, Park et. al. developed a physical model of film growth rate in ALE within the conceptual framework of fractional coverage exchange [8]. Equation 2 provides an explicit relation between the coverage exchange fraction f and the film thickness per deposition cycle d_c [8]. The growth rate may be derived from dividing d_c by the sum total of species injection and purging pulse length [8]. Note here α^{AB} is a lumped factor that accounts for all effects that may result in the discrepancy between adsorbate and atomic coverages, including the purging re-evaporation and steric hinderance mentioned previously. $\bar{\theta}^{AB}$ can be considered as the coverage extent that subsequent adsorbate species have on its immediate preceding layer [8]. Moreover, the processing conditions such as temperature and partial pressure affect $\bar{\theta}^{AB}$ through the adsorption and desorption coefficients in the Langmuir adsorption isotherm differential equation [8].

$$d_c = \frac{f^{AB} f^{BA}}{1 - g^{AB} g^{BA}}, \text{ where } g^{AB} = 1 - f^{BA} = 1 - \alpha^{AB} \bar{\theta}^{AB}$$

(Equation 2)

Another property worth investigating is the atomic layer morphology as it plays a crucial role in determining the success of subsequent processes and the eventual device performance. Depending on the degree of lattice mismatch and deposition layer thickness, epitaxial growth mode can be roughly classified into three categories: Frank van der Merwe (FM), Stranski-Krastanov (SK) and Volmer-Weber (VW). The FM mechanism is observed in heteroepitaxial auto-epitaxial systems with very low lattice mismatch where growth takes place in 2D through either island or step formation. This is considered the ideal case for thin film growth [9]. As the layer thickness grows, three dimensional islands form atop a thin film fully-covered the substrate; this referred to as the SK morphology. Two well-documented SK examples are the Ge/Si(100) and In_xGa_{1-x}As/GaAs(100) systems [10]. To understand whether such structure represents the ground state or simply a metastable phase enroute to a flat arrangement, Ratsch et al. developed an equilibrium model based on the principle of Frenkel-Kontorova (FK) energy minimization [10]. Equation 3 shows the total energy for all vertically coupled chains at zero Kelvin [10]. E_R is the total relaxed island energy, which is a sum of FK energy in all layers [10]. N_p is the number of saturation molecules on the p^{th} layer and h is the total number of layers [10]. E_{FK} is dependent on the

relative periodicity a_p adjusted based on its previous layer and the relative displacement value ε_p under the assumption that every chain is imagined to interact with the rigid substrate [10]. The maximum width of simulated ALE islands was reported to agree with scanning tunnelling microscopy observations [10]. In the last case of VM, the mechanism applies in highly-mismatched systems where island growth is observed directly on the substrate without wetting layers. Since SK growth can be considered the special case of VM and FM growth at the limit of wetting layer critical thickness approaching zero and infinity respectively, Lozovoy et al. solved the expression for change in free energy upon island nucleation, taking into the substrate surface, strain relaxation and atomic attraction terms, obtained the dependence of growth regime on critical thickness and lattice mismatch at a given temperature, as shown in Figure 2 [9].

$$\begin{aligned}
 E_{tot} &= E_R - \sum_{p=1}^h (4N_p + 2)E_{bond} + \frac{1}{2}hE_{dimer} \\
 E_R &= \sum_{p=1}^h E_{FK}(N_p, a_{p-1}) \\
 a_p &= a_{p-1}\left(1 + \frac{\varepsilon_p(N_p) - \varepsilon_p(1)}{N_p - 1}\right)
 \end{aligned}
 \tag{Equation 3}$$

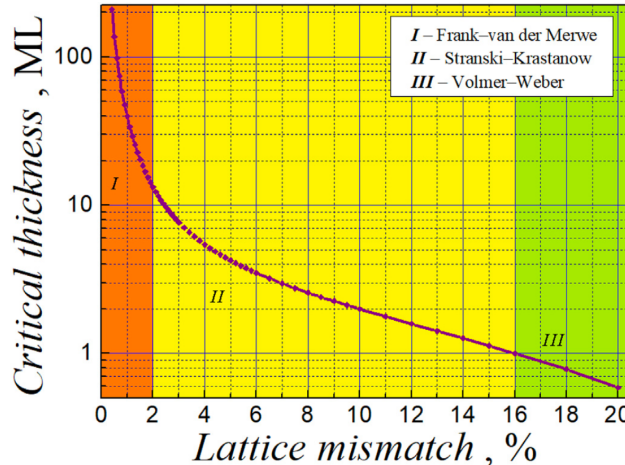


Figure 2. Dependence of the critical thickness for 2D-to-3D transition on lattice mismatch at $T = 450^\circ\text{C}$ [9]

Theoretical discussions aside, many instruments have been demonstrated to be helpful for characterizing the underlying atomic mechanisms in ALE processes. For instance, *in situ* X-ray scattering have been used to study ZnSe growth on GaAs substrates [11]. From diffraction data, many properties of the thin

film such as long-range structural order and the epitaxial stress evolution can be deduced from bond reconstruction and line analysis [11]. In addition, reflection high-energy electron diffraction (RHEED) has been used to monitor growth conditions including substrate temperature and reagent pressure [12]. From spectral beam intensity and phase data, surface stoichiometry of the thin film may also be estimated [12].

4.0 Processes

4.1 Substrate Preparation

Before any epitaxial process, the wafer substrate must be cleaned to create a surface without any defect or impurity. Trace impurities can be especially detrimental on semiconductor surfaces as they can diffuse into the substrate and cause defects during high-temperature processes. The seemingly basic requirements of cleaning can be difficult to fulfill as atoms will always move to reconstruct a surface with a minimal number of dangling bonds. To prevent ambient oxidation, the cleaning process is usually carried out in an ultrahigh vacuum environment. Thin oxides may be removed by the RCA process while organic residuals may be removed by SC1 followed by an HF recovery step. The HF dip creates a passivated surface with Si-H bonds which desorbs at about 500°C [13]. For adsorbed organics, UV-ozone has been demonstrated to be generally effective. The chemistry of wafer cleaning has remained more or less the same for the past 50 years, but its implementation has changed with optimized equipment. Most notably, to meet the high throughput demand of the modern electronics industry, companies such as FSI Corporation and CFM Technologies have developed automated systems as early as 1975. Besides the most popular chemical immersion based methods, physical techniques such as brush scrubbing, fluid jet, ion bombardment and high-intensity ultrasonic are alternative techniques for cleaning but are generally avoided whenever possible to minimize surface damages that may be irreparable without high temperature annealing [14][15].

Some modifications to the RCA have been proposed to reduce waste handling, save cost and increase cleaning efficacy. By adding tetramethylammonium hydroxide (TMAH) and ethylenediaminetetraacetic acid (EDTA) to the RCA SC-1 cleaning solution, Pan et al. showed that the standard hydrochloric acid / hydrogen peroxide / water mixture (HPM) step may be omitted without compromising wafer surface smoothness and even improving the electrical properties of subsequent metal oxide layer [16]. Akiya et al. demonstrated that adding chelating agents into the SC-1 solution could reduce metallic contamination [16]. To address the environmental issues of RCA, Ryoo et al. have reported on electrolyzed ultrapure

water as an alternative for wafer cleaning [17]. The anode water and cathode water have a lifetime around 40 minutes, sufficient for the cleaning process, then deteriorate due to CO₂ and O₂ saturation respectively [17]. Most importantly, the consumption of chemicals with electrolyzed water is 1/10 times less than that of RCA [17]. To be concrete, in order to clean 8-inch wafers, RCA utilizes 91 types of chemicals while electrolyzed water only consumes 600 mL of NH₄Cl with a similar cleanliness outcome [17].

4.2 Solid Phase Epitaxy

Solid phase epitaxy (SPE) refers to the local bond rearrangement process within which a metastable amorphous material occurs, facilitated by thermal heating or laser irradiation, when placed in contact with an underlying crystalline substrate template. The amorphous material is converted into a crystalline layer by layer with rates more than 100 $\mu\text{m}/\text{s}$ reported [18]. The growth rate can be measured using the time-resolved reflectivity method, making use of the difference in refractive index across the interface [18]. Although SPE does not involve cycles of surface-limited reactions, it technically still qualifies as atomic epitaxy and warrants a discussion herein.

Theoretically, SPE may be modelled by a simple Arrhenius-type equation while experimental results have revealed more nuanced complications about the process with orientation, pressure and dopant dependence. For instance, the SPE growth for Si on a (001) crystal plane can be 25 times faster than that of (111) while the activation energy stays the same [18]. In addition, (111) growth tends to result in a significantly higher density of defects [18]. Moreover, the growth rate of Ge experiences an exponential enhancement with hydrostatic pressure and III/V type dopants amplify this effect [18]. It is worth noting that non-doping impurities such as hydrogen atoms generally retard the interface motion, suggesting the process's sensitivity to shift in the Fermi level [18]. Johnson et al. has published a comprehensive review on the crystallization behavior of Si and Ge materials using SPE [18].

To fully appreciate the atomic intricacy at the amorphous crystalline interface, molecular dynamic simulation is a powerful tool to visualize the SPE process. For instance, to simulate Si SPE, Motoooka et al. first constructed a $21.7 \times 21.7 \times 43.4 \text{ \AA}^3$ tetragonal prism cell with 1024 Si atoms to match the material density [19]. Specifically, eight $c - \text{Si}$ (001) layers were then placed in contact with a block of bulk $\alpha - \text{Si}$ obtained from rapid quenching of liquid Si [19]. Finally, the cell was heated to various temperatures 1450~2000 K for SPE with the atomic movement governed by the Langevin integrator in Equation 4 [19]. Here, $r_i(t)$, $F_i(t)$ and $R_i(t)$ are the position vector, interatomic force from Tersoff potential and random force for temperature control respectively for atom i at time t . m and γ are the

atomic mass and friction constant [19]. A typical molecular dynamic simulation results for SPE is shown in Figure 3 where the gradual crystallization of Si atoms over time at 1800 K is evident [19]. The author was also able to conclude that the flat (001) interface grows rougher with (111) facets as the annealing temperature increases as well as to extrapolate temperature-dependent activation energies from growth rates [19]. Similar molecular dynamic simulation has also been reported for Ge SPE, but using a Stillinger-Weber type interatomic potential [20].

$$m\ddot{r}_i(t) = F_i(t) - m\gamma\dot{r}_i(t) + R_i(t)$$

(Equation 4)

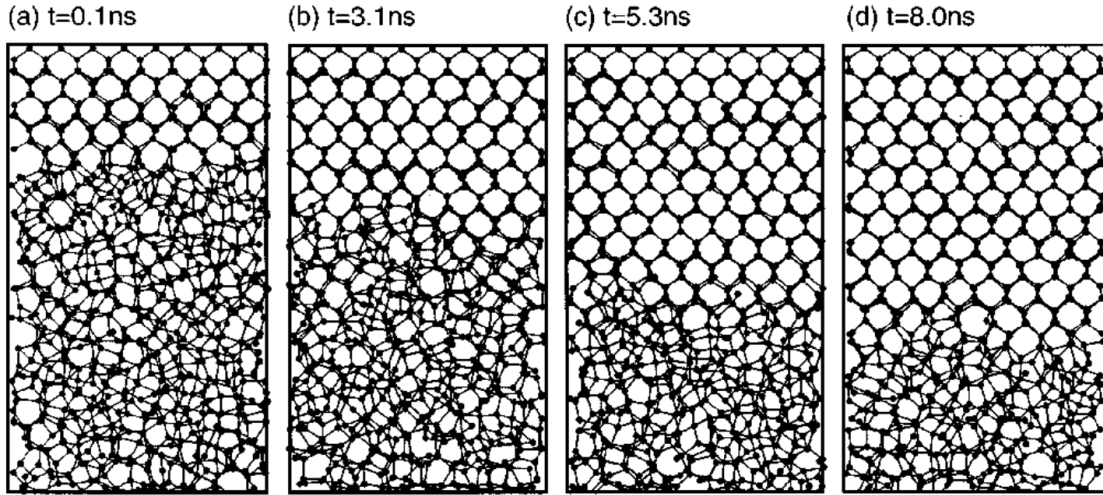


Figure 3. Molecular dynamic simulation of Si SPE at 1800 K [19]

Besides its important role in the crystallization of Si and Ge, SPE has also been utilized in fabricating high quality silicide contacts, dielectrics and semiconductors, thus rendering it an integral part of the CMOS processes. SPE of palladium, platinum, nickel, chromium, iron, cobalt, titanium vanadium and rhodium silicide has been reported in extensive reviews [21][22][23]. For its application in dielectric fabrication, Toyoda et al. demonstrated the effects of SPE annealing on delivering a sharp and abrupt interfacial conduction band discontinuity, which translates to high insulation performance under voltage overdrive, for a Al₂O₃ gate insulator film on GaN [24]. For SPE in semiconductor fabrication, a recent noteworthy advance was the incorporation of GeSn channel in Si CMOS reported by Maeda et al. GeSn has long been predicted as an alternative channel material for high speed Si CMOS technology but is unfortunately limited by poor defect density due to large lattice mismatch [25]. Maeda et al. reported on

ultrathin crystalline GeSn layers on Si (111) substrates by SPE annealing in N₂ ambient to limit adatom surface mobility [25]. The device showed ideal transfer characteristics and superior 90% hole mobility enhancement compared to the pure Ge channel on Si, realizing the promise of GeSn CMOS and proving the effectiveness of SPE processes [25].

4.3 Liquid Phase Epitaxy

Liquid phase epitaxy (LPE) refers to the process of depositing metal coordination and organic linker precursors in an alternating fashion, acting as chemical “struts” and “joints” respectively, on a functionalized substrate, serving as a template for nucleation sites and a guide for growth orientation, to obtain metal-organic thin films (MOTFs) with high homogeneity and low roughness [26]. Figure 4 shows the conceptual layer-by-layer preparation of SCP systems [27]. The film begins with the nucleation of small isolated nano-crystallites on the seeding layer following the VW growth mechanism. As the deposition cycle continues, the existing crystallites grow and collide with each other to cover up the underlying substrate. New nucleation events remain possible but become less likely due to the drastically shrinking accessible substrate area. Next, a layer of metal ions populates the exposed coordination sites, followed by a bridging layer of organic molecules protruding upward presenting an interface for subsequent cycles. The nucleation process occurs faster for samples prepared at higher temperatures with preferential lateral growth, resulting in accelerated surface coverage and reduced surface roughness. Ohnsorg et al. demonstrated that for carboxylic acid terminated self-assembled monolayers on gold, the crystal orientation leaned more towards (111) over (100) at 50 °C than 25 °C, revealing another temperature dependency of the LPE process [28]. Further, chemical functionality of the SAM layer has also been reported for its influence over MOF crystallography. For instance, CH₃-terminated SAM can completely suppress MOF growth while SH-group at α position makes not only deposition possible but also controls orientation of the deposited film [29].

The sequential stepwise approach theoretically allows the interposition of different MOTFs one on top of another, thus achieving hybridized selective functionalization. The first crystalline product from LPE was [Cu₃(btc)₂]_n grown on -COOH and -OH terminated self-assembly membrane on gold substrate, by alternating the copper acetate and benzene 1,3,5-tricarboxylate moieties with intermittent ethanol rinsing. One remarkable feature of MOTFs is its extreme porosity with Langmuir surface of 10400 m²/g [26]. Other inorganic compounds including anatase, zeolites, calcium carbonate, zinc and iron oxides have also been successfully grown [30]. In addition, LPE processes enable post-synthetic modifications which renders it an attractive technique in the fabrication of smart membranes, chemical sensors and drug

deliveries [31][32][33]. Common MOTF preparation techniques include solvothermal growth, gel-layer synthesis, evaporation-induced crystallization and microwave-induced deposition [26]. To meet the demand for spatially defined MOTF deposition, patterning techniques such as electron-beam lithography and inkjet printing have also been developed [34]. Zhuang et al. have published a comprehensive review on the recent development of LPE [35].

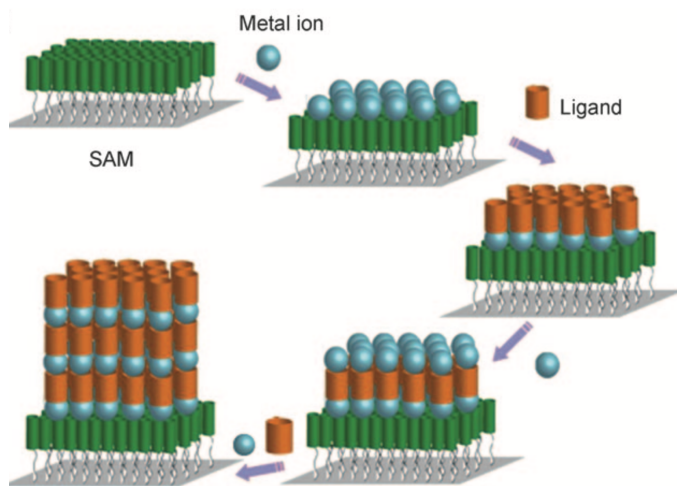
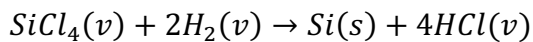


Figure 4. Layer-by-layer preparation of SCP systems [27]

4.4 Vapor Phase Epitaxy

Vapor phase epitaxy (VPE) of silicon has become an essential part of integrated circuit technology since the 1970s. VPE grows a lightly doped layer on top of a heavily doped substrate from which MOSFETs can be built. The substrate's function is to short the lateral parasitic devices and thus eliminate latch-up. Further, VPE Si layers have significantly lower concentrations of carbon and oxygen contaminants compared to the industry standard Czochralski wafers. A typical silicon VPE barrel reactor is shown in Figure 5 [36]. The main advantage of epitaxial wafers is the capability of adjusting the dopant profile in vertical direction without causing any damage or defect as in the case of high energy ion implantation technique. Silicon VPE is commonly carried by the reducing chlorosilanes delivered through a H₂ bubbler. Note that the bubbler pressure is adjusted to maintain a constant volume ratio required for consistent growth [37]. The dominant growth species are SiCl₄ and SiCl₂ at low and high temperatures respectively [37]. SiCl₄ is a common by-product of polysilicon process, which can be purified and is available in large quantity at low cost [37]. As evident from the chemical Equation 5, the release of HCl indicates that the VPE process involves a balance between growth and etching [37]. In other words, the degree of process

reversibility increases with the chlorine content [37]. Nevertheless, $1 \mu\text{m min}^{-1}$ growth rate can be achieved with SiCl_4 in spite of the low degree of supersaturation intrinsic to the process [36]. High growth rate of $40 \mu\text{m min}^{-1}$ has been achieved by HCl-assisted pyrolytic decomposition of silane [37]. But the process can occur homogeneously in the gas phase when the chamber temperature exceeds 400°C , thus deposition on the reactor wall is unavoidable [37]. The mandatory cleaning limits the overall productivity. Growth by disproportionation reaction involving the dissociation of divalent silicon halides, including SiI_2 , SiCl_2 , SiBr_2 and SiF_2 , is also feasible and particularly desirable as it can be carried out at near equilibrium, a condition ideal for selective epitaxy [37]. However, the process requires a closed system, inconvenient for dopant incorporation [37]. Therefore, chlorosilane reduction remains the most popular of all three processes mentioned above.



(Equation 5)

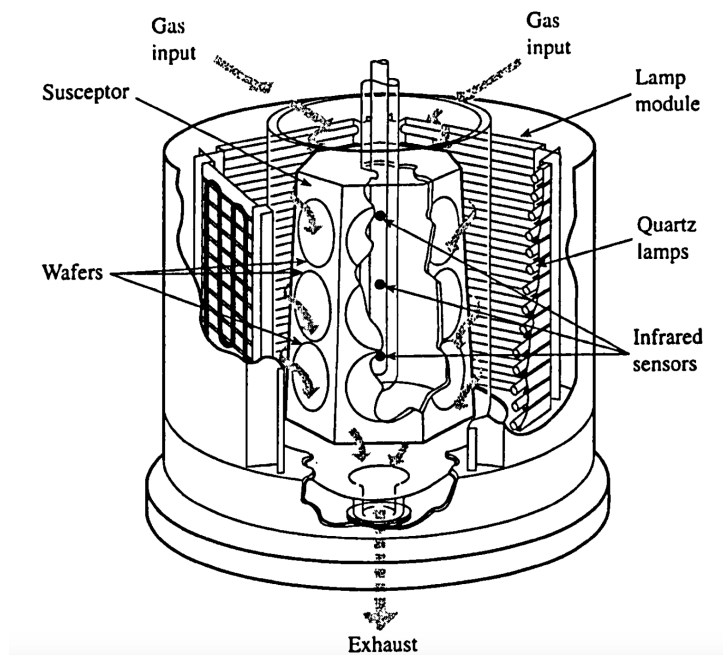


Figure 5. A silicon VPE barrel reactor [36]

A simple model for the VPE is described by Deal where the deposition species flux across a gaseous boundary is set equal to that of reactant consumption by growth. This is shown in Equation 6, where h_g is the mass transport coefficient, k_s is the surface reaction rate, C_g and C_s are the species concentrations in the gaseous phase and on the wafer surface respectively. The growth rate can thus be approximated

by R . It is worth noting the mass transport limited regime occurs when $k_s \gg h_g$ and the reaction rate limited regime occurs when $h_g \gg k_s$. The Deal-Grove model grossly oversimplifies the growth process as it does not account for all the competing chemical reactions taking place at the surface [38][13].

$$F = h_g(C_g - C_s) = k_s C_s$$

$$R = \frac{k_s h_g C_g}{(k_s + h_g)N}$$

(Equation 6)

Apart from Si deposition, organometallic vapor phase epitaxy (OMVPE), named after the compound precursor, is also a popular subclass of VPE for semiconductor growth. The earliest patent for OMVPE dates back to 1954, when Scott et al. filed for the growth of InSb using triethyl-indium and stibine [39]. The late 1960s saw the pioneering publications of Manasevit and coworkers on the single-crystalline layers of III/V, II/VI and IV/VI materials [39]. By 1975, any doubt about the purity of OMVPE semiconductors was dispelled when the low-temperature mobility of GaAs exceeded $100,000 \text{ cm}^2/\text{V} \cdot \text{s}$ [39]. Today, OMVPE has demonstrated success in depositing a wide array of materials, aside from the aforementioned semiconductors, also nitrides and oxides with a wide range of applications from light emitting diodes to solar cells [40][41][42][43][44]. Generally, in OMVPE, reactants take turns to be transported by a carrier gas to the reaction chamber, where decomposition of the organometallics may occur. It is common for the growth rate to be limited by the nucleation of metallic layers. The underlying mechanism for OMVPE growth is incredibly complex, involving thermodynamics, hydrodynamics, kinetics, mass transport, surface chemistry and sub-surface processes. Hence it is usually determined on a case by case empirical basis and the research community has virtually abandoned the hope of modeling it. Stringfellow has written a comprehensive review covering the various sub-processes in OMVPE growth, thus the efforts will not be duplicated in this report [45]. Although there is any adequately accurate model for OMVPE, the bottom line is that the process induces structural changes in the overlayer which result in the differentiation between surface and bulk structures. *In situ* X-ray measurements can reveal important details about the underlying OMVPE process. For instance, the peak intensity evolution may be indicative of epitaxial strain relaxation accompanied by the introduction of misfit dislocations and spectral reflectivity fluctuation may help us determine the saturation of an organic or metallic element at a given moment [11].

4.5 Molecular Beam Epitaxy

In molecular beam epitaxy (MBE), the reactants are impinged straight onto the substrate by molecular beams under ultrahigh vacuum conditions. As a result, the need for high temperature gas carrier observed in OMVPE may be eliminated. Historically, the MBE process was discovered from conducting a surface vapor interaction study using the latest mass spectrometer in the 1960s [46]. In 1969, Cho demonstrated the successful fabrication of GaAs-Al_xGa_{1-x}As laser structure which was considered a crucial test for any III-V process [46]. Four years later, Chang et al. reported on observing the theoretical resonant tunneling effect in a superlattice structure grown from alternating GaAs and AlGaAs using MBE [46]. Within a short time, MBE became an established research tool for ALE and solid state physics [46]. Figure 6 shows a schematic and a photograph of an MBE system. The crystallization process is facilitated by the reactions between the molecular beams and the outermost atomic layer of the substrate surface, which is maintained at an elevated temperature to provide thermal energy for adatom migration. The epitaxial layer composition and its doping level is determined by the relative arrival rates of the constituent elements and dopants, which intuitively depend on the evaporation fluxes [47][14].

Coupled with the utilization of mechanical shutters, the transient effects from diffusion during cycling is significantly reduced for ALE growth using MBE. The interlock system allows substrates to be introduced into the growth chamber without breaking vacuum. In addition, an MBE machine is usually equipped with other analytical facilities to monitor the growth process. A quadrupole mass spectrometer may be used for residual gas analysis, a reflection high-energy electron diffraction arrangement may be used for surface assessment and an Auger electron spectrometer may be used to compositional study. The growth rates for MBE are in the range of $0.1\sim10.0 \mu\text{m } h^{-1}$, which correspond to beam fluxes from $\sim5\times10^{13} \text{ atoms cm}^{-2}\text{s}^{-1}$ to $\sim5\times10^{15} \text{ atoms cm}^{-2}\text{s}^{-1}$ [14]. Three most commonly used source types in MBE are solid source effusion cells, also known as Knudsen cells. For Knudsen cells, the beam intensity is temperature controlled following Equation 7, where J_i is the atomic flux per unit area of mass m_i , through an aperture of area a , at a distance of d , from angle θ under partial pressure p_i [14]. To simplify the calculation, the source flux is assumed to have a cosine distribution with its peak aligned with the cell's central axis. Note that this distribution only holds when the cell is relatively full. As the source material depletes, the collimating effect from the crucible walls becomes more pronounced [48]. Since the flux is inversely proportional to the squared cell-to-wafer distance, the cell is placed 5~8 inches away to maximize J_i without compromising deposition uniformity [48]. Since the substrate

temperature and deposition rate are usually fixed in conventional MBE, the process is often combined with an annealing step after growth to improve the film quality [5].

$$J_i = \left[\frac{ap_i}{\pi d^2 (2\pi m_i k_B T)^{1/2}} \right] \cos\theta$$

(Equation 7)

The growth model for mono-component MBE system developed by Burton, Cabrera and Franks (BCF) paints a deterministic step-flow picture. The BCF theory states that when an adatom reaches the substrate surface, it has to diffuse to the closest kink site on a growing edge, which acts as a capturing sink [13]. Crystal growth occurs as the terrace edges sweep across the wafer. Mathematically, the BCF theory formulates a relationship between four critical variables: λ_s , the migration length, n_s , the surface density and σ , the supersaturation parameter in Equation 8 [13]. It is worth noting that the model ignores nucleation and assumes the surface step moves slowly. Further, the capture probability of approaching a step from above and below cannot be identical due to the inherent structure asymmetry during growth. Therefore, BCF implies a discontinuity in the concentration distribution of adatoms when the step moves fast [49].

$$\lambda_s^2 \nabla^2 n_s + n_s = n_{s,eq}(\sigma + 1)$$

(Equation 8)

In practice, III-V compounds are commonly deposited by MBE and the lateral dimensional control is achieved by oxide masks or shadow masks. Further, MBE is frequently applied for semiconductor and dielectric junction formations due to its ability to deposit multiple materials in a single cycle without breaking vacuum [50]. Because its precision in the growth direction can be as small as the atomic spacing, MBE has also been used in the fabrication of quantum structures for nanoelectronics devices and for theoretical studies. For instance, a quantum well can be created by sandwiching a GaAs thin film between two $\text{Al}_x\text{Ga}_{1-x}\text{As}$ barriers. Mata et al. have published a comprehensive on MBE grown 0D, 1D and 2D quantum structures [51].

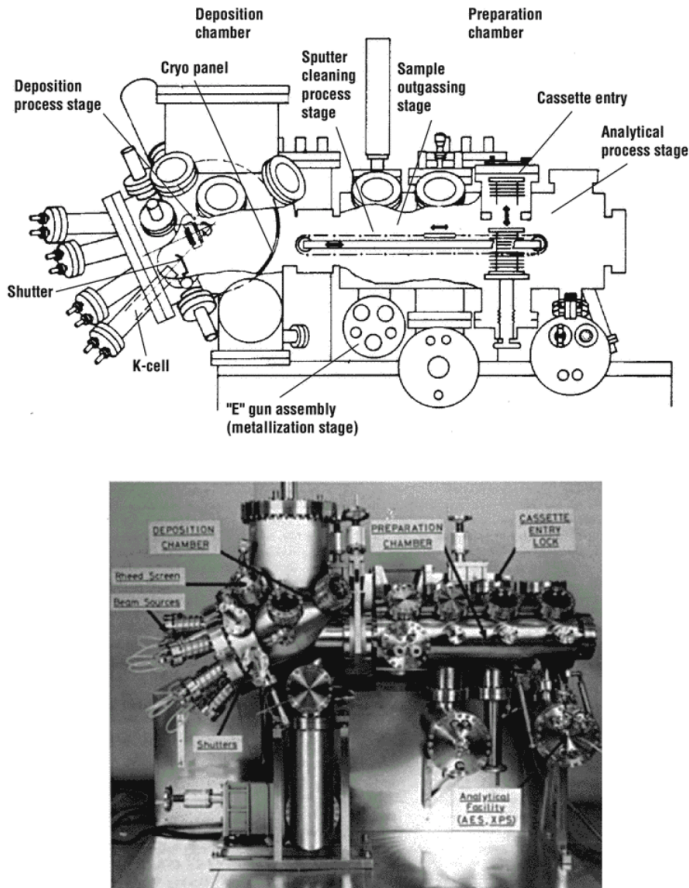
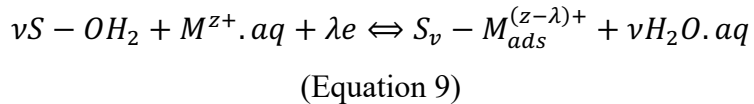


Figure 6. Schematic and photograph of a typical MBE system [13]

4.6 Electrochemical Epitaxy

Vacuum ALE processes often involve high precision machineries that are expensive to acquire. On the other hand, electrochemical ALE (ECALE), which takes turns with the underpotential deposition (UPD) of each compound element, hold great promises as an affordable room-temperature growth alternative [52]. Herein, ECALE is classified as a type of ALE because under the special condition of UPD, deposition exhibits anomalous behaviours in the sense that as soon as the substrate has been covered, the process stops, an apparent violation of Nernstian electrochemistry [52]. No subsequent deposition is possible unless the metal ions somehow diffuse through the monolayer barrier like oxygen molecules do in silicon oxidation. But that does not seem to be the case in many research papers. UPD refers to the deposition of a usually less noble metal on a more noble one at a potential lower than what is required for bulk formation of the former. The phenomenon occurs when the binding energy of an adsorbed metal atom on a foreign surface is higher than that to itself [53]. During UPD, a metal ion first penetrates into the double layer and establishes contact with the substrate metal. This step is accompanied by the removal

of previously adsorbed water molecules and the disruption of solvation shell [53]. Then, if a chemisorption bond is formed between the adsorbent and adsorbate, the partial charge transfer of electrons will take place. Kinetically, besides the obvious steps of transport, transfer and adsorption, nucleation and diffusion on the substrate surface also play a crucial role in the monolayer formation. Essentially, the process can be described by the chemical reaction in Equation 9, where λ and v are partial charge transfer coefficient and electro-adsorption valency respectively [53].



In ECALE, elements are frequently flushed in through capillary action and rinsed out by an ultrapure electrolyte; this draws parallel to the various shutters and purging gases in MBE. The electrochemical cells are configured to maximize surface-to-volume ratio to reduce contamination and the substrate material is carefully selected to avoid lattice mismatch strain. Common substrate choices include Au, Pt, Ni and Cu [54]. The most significant drawback of ECALE is its deposition rate. Given that each cycle would require about fifteen operations, deposition of over ten cycles can become rather tedious [55]. To tackle this issue, automated systems such as thin-layer flow cell and H-cell have been proposed as shown in Figure 7. Thin-layer flow cells resemble electrochemical detectors in chromatography machines. They are simple to use and generate little waste but suffer from low reproducibility due to trapped bubbles and edge effects. In comparison, the performance of H cells is more consistent because substrates are hung on the Pyrex body and precursors alternates through flushing. To reduce the oxygen contamination drawn in from solution exchanges, the system should be contained in a nitrogen purged box [56][57].

Both II-VI and III-V semiconductor materials have been successfully grown with ECALE including GaAs and CdSe, which are commonly used in optoelectronics. Villegas et al. demonstrated the ECALE of GaAs on Au(100) surfaces [58]. Arsenic was first deposited from 1.0 mM $HAsO_2$ 1.0 mM H_2SO_4 solution at pH 3.2 and subsequently reduced in buffered 10.0 mM Cs_2SO_4 at pH 4.7 at -1.25 V [58]. Then the As-covered surfaces were immersed in 0.5 mM $Ga_2(SO_4)_3$ at pH 2.7 at -0.71 V for Ga deposition [58]. Colletti et al. demonstrated the ECALE of CdSe on Au covered Si(100) wafers. Se was deposited and stripped at -0.6 V and -0.8 V respectively from 5.0 mM $HSeO_3^-$ obtained from SeO_2 in 5 mM acetate buffer at pH 4.5 [55]. Cd was subsequently deposited at -0.55 V from 5.0 mM $CdSO_4$ in 50 mM acetate buffer at pH 5.7 [55]. Recently, ECALE has also been applied in the fabrication of CdS, CdTe and CdSe quantum dots to sensitize the TiO_2 nanorod array based photoelectrodes, demonstrating

its excellent control over microstructures; the photovoltaics devices showed power conversion efficiencies of 6.57%, 7.90% and 4.08% respectively [59][60][61]. Superlattice structures made from ECALE have also been reported [62][63][64].

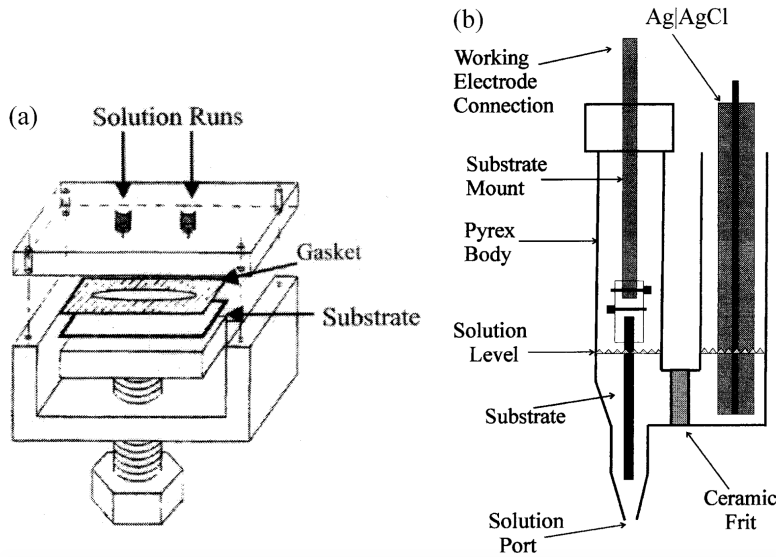


Figure 7. Two common ECALE systems: (a) thin layer flow cell (b) H cell [56]

5.0 Applications

The precise control of ALE has made it increasingly popular in microfabrication compared to traditional methods as the feature sizes continue to shrink according to Moore's law. This final section places its emphasis on applications of ALE including transistors, optics, displays, solar cells and medical devices. ALE has been applied in the fabrication of many components of a transistor. ALE HfO_2 has been grown from alternating pulses of HfCl_4 and H_2O , tested as a gate oxide for potential InGaAs transistors [65]. ALE AlN has been grown from trimethylaluminum at the interface of a AlGaN/GaN transistor for passivation to replace the leaky PECVD SiO_x [66]. Perhaps the most exciting application of ALE in the past decade, in the author's humble opinion, came from Lin et al., who reported a graphene-based transistor fabricated from wafer-scale epitaxy [67]. The device achieved stable operation at 100 GHz under a drain bias of 2.5 V with a gate length of 240 nm, more than twice of the 40 GHz frequency commonly observed in conventional Si metal-oxide semiconductor transistors [67]. The atomic graphene layer was epitaxially formed on a high purity SiC wafer by thermal annealing at 1450 °C and an interfacial layer made of poly-hydroxystyrene derivatives was spin-coated on it to promote HfO_2 gate adhesion [67]. The graphene layer was measured to have an extremely high electron carrier density of $3 \times 10^{12} \text{ cm}^{-2}$ and a Hall-effect mobility of $1000\text{--}1500 \text{ cm}^2\text{V}^{-1}\text{s}^{-1}$, which undoubtedly contributed

to its high-frequency operation performance [67]. Although the original paper did not disclose experimental details of the graphene growth, it is assumed that the process was carried out using MBE, whose success with graphene ALE had been reported in multiple papers [68][69][70].

In copper indium diselenide solar cells, a buffer layer, most commonly CdS, is usually inserted between the window and the absorber to facilitate charge extraction and mitigate stress-induced degradation [71]. However, there is great interest in replacing cadmium-based buffers with In_2S_3 for environmental reasons. Yousfi et al. grew indium sulfides using ALE, which was shown to consistently outperform their sputtering counterparts in terms of the yield, FF , I_{SC} and V_{OC} . This was expected since insufficient protection would lead to surface damage during sputtering. A 50 nm In_2S_3 prepared by ALE had a 10% yield, 65% fill factor, 30 mA/cm^2 and 515 mV [72]. The thin film was also reported to have a bandgap of 3.25 eV, significantly higher than that of its bulk material [72]. This is highly desirable as a high bandgap buffer would allow increased collection in the UV range. Table 2 shows buffer layers of different compositions processed by ALE and sputtering for comparison in terms of FF , I_{SC} and V_{OC} [72]. Besides buffer layers, ALE has also been used for the deposition of many solar cell components ranging from front contacts to heterojunction absorbers as tabulated in Table 3 just to list a few [73].

Table 2. Performance comparison of ALE & sputtered buffer layers [72]

Buffer	Thickness (nm)	ALE	Sputtering
TiO_2	20	9 mA/cm^2 , 305 mV, 23%	24.2 mA/cm^2 , 214 mV, 47.7%
Ta_2O_5	2	24.5 mA/cm^2 , 406 mV, 40%	27.6 mA/cm^2 , 245 mV, 49%
In_2S_3	30	30 mA/cm^2 , 505 mV, 61%	27 mA/cm^2 , 409 mV, 55%
ZnO	30	25.5 mA/cm^2 , 505 mV, 69.5%	26.6 mA/cm^2 , 240 mV, 45%
Al_2O_3	1	30 mA/cm^2 , 572 mV, 53%	32 mA/cm^2 , 45 mV, 27%

Table 3. ALE in solar cell applications [73]

Solar Cell Types	ALD Materials	Applications	ALD Chemistry
$\text{TiO}_2/\text{Cu}_x\text{S}$ heterojunction	$\text{Cu}_{1.8}\text{S}$	absorber film	$\text{Cu}(\text{thd})_2 + \text{H}_2\text{S}$
PERC-type a-Si	Al_2O_3	surface passivation	$\text{Al}(\text{CH}_3)_3 + \text{O}_2^{\text{plasma}}$
a-Si thin film	ZnO	front contact	$\text{Zn}(\text{C}_2\text{H}_6)_2 + \text{H}_2\text{O}$

Besides the abundant reporting of light emitting diodes with quantum wells, ALE has also been applied to other areas of the display technology [74][75][76]. Ta₂O₅ is often used as an insulating layer in electroluminescent displays due to its high breakdown strength. However, high permittivity also lowers the Poole-Frenkel conduction barrier, increasing the leakage voltage [77]. To resolve this issue, Kukli demonstrated a novel ZrO₂/Ta₂O₅ nanolaminate with a remarkable charge-storage factor of 64 nC/mm², a metric describing the charge stored per unit surface area at 1 μA/cm² leakage [77]. Using ALE, the nanolaminates was grown by alternating the exposures of 0.2 s Ta(OC₂H₅)₅ + 2.0 s H₂O and 0.2 s ZrCl₄ + 0.5 s H₂O at 325 °C [77]. The superior electrical performance of ZrO₂/Ta₂O₅ was attributed to the nanosized crystallites of metastable ZrO₂, which increased the number of boundaries and decreased the probability of stumbling upon breakdown-level voltage at gain weak points [77].

The application of ALE is not limited to the world of electronics. Traditionally optical thin films are fabricated using evaporation or sputtering techniques. To reduce film porosity and increase interface uniformity, Riihelä et al, demonstrated optical thin film deposition using ALE, using Fabry-Perot filters as an example [78]. Fabry-Perot filters of 20 quarter-wave layers were fabricated by alternating AlCl₃/ZnCl₂ and H₂O/H₂S flow on glass, spaced with N₂ purging [78]. Compared with the theoretical ideal structure, the peak transmittance was observed to have been reasonably well reproduced in the experimental spectra [78]. In addition, nuclear resonance broadening measurements showed that the hydrogen content was around 0.1%, a confident indication of high film density. [78] However, experiment showed that side-band regions around the peak deviated from target values. [78] The author attributed this to the thickness discrepancy in the uppermost part of the Fabry-Perot multilayer structure and recommended replacing the crucible solid source with alkyl compounds such as trimethyl aluminium as a solution [78]. The only drawback about ALE seemed to be its efficiency, referring to the 0.39 Å and 0.79 Å growth rate per cycle for AlCl₃ and ZnCl₂ respectively [78]. Nevertheless, ALE can still achieve reasonable competitiveness in terms of its productivity when it comes to film volume per unit time [78]. ALE has also been applied to fabricate photonic crystals where only certain frequencies of light selected by the bandgap are allowed to propagate. The 3D structure was achieved through infiltrating an opal template with high dielectric materials to fill the interstitial voids [79]. The template is then etched by acid to expose an inverted lattice of spheres [79]. King et al. successfully infiltrated silica thin films using TiCl₄ and H₂O as ALE precursors [79]. The resulting TiO₂ deposition exhibited high crystallinity and strong photoluminescence [79].

In the field of controlled release, nanostructured materials are playing an increasingly prominent role in smart drug delivery. This is because often systemic administration of chemotherapeutic agents is plagued

by significant side effects and many DNA-based treatments have relatively short *in vivo* activities. Traditional fabrication methods such as ion etching and electrochemical corroding result in wide pore size distribution and thus inconsistent performance for nanostructures. To overcome this issue, Narayan et al. reported the use of ALD for pore size control in alumina membranes through TiO₂ coating [80]. Figure 8 shows an SEM image of a nano-porous alumina membrane following ALD deposition of 8nm TiO₂ [80]. The process involved alternating exposures to titanium tetrachloride and water vapor at 300°C and a growth rate of 0.86~1.0 Å° was achieved [80]. The high-resolution SEM of the alumina membrane surface revealed TiO₂ nanocrystals with lateral dimensions of ~20 nm [80]. Human epidermal keratinocyte viability assayed by MTT showed no compromise in its viability and the nanostructure showed evident antimicrobial capability likely due to the photocatalysis generated peroxidation of the *E. coli* phospholipid membranes [80]. In summary, ALD has been demonstrated to be an effective tool to control the pore size of nanostructures in biomedical applications.

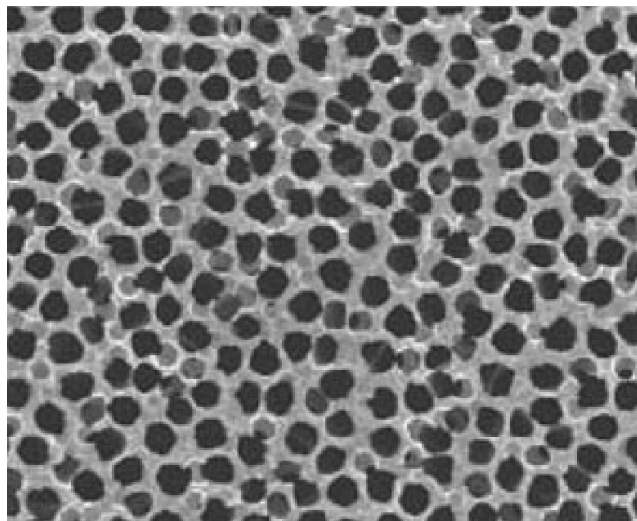


Figure 8. ALD controlled nano-porous alumina membrane [80]

5.1 Quantum Structures & Superlattices

To grow any quantum nanostructure, control over its composition, shape and doping with atomic precision is imperative. Nanostructures including quantum wires and dots are highly sought after in optoelectrical applications. Briefly, quantum wires are desirable for their large sub-band density of states, which translates to high differential gain in lasers [81]; and quantum dots are desirable for their multiple exciton generation capability, which translates to high energy conversion efficiency in solar cells [82]. MBE has been demonstrated effective at growing quantum wires of semiconductor materials such as

SiGe and InGaAs with the help of V-groove patterned substrates for geometry control [83][84]. For example, Isshiki et al. successfully fabricated $10\text{ nm} \times 35\text{ nm}$ GaAs_{0.8}P_{0.2} nanowires using TMG, AsH₃ and PH₃ sources [85]. The quantum wire was grown in a V-shaped GaAs groove with a (100) base and (111) side walls [85]. Switching mode technique was implemented to impose geometry control over the quantum wire, taking advantage of the fact that crystallographic selectivity may be easily regulated by hydrogen purge time [85]. In addition, infrared irradiation using a halogen lamp was incorporated into the overall process to eliminate surface methyl group and thus reduce carbon contamination level [85]. The growth sequence is shown in Figure 9 [85]. Similarly, MBE has been successful at growing quantum dots, too, including Ge/Si, Sn/Si, InAs/GaAs etc. [86][87][88]. Mukai et al. demonstrated $In_{0.5}Ga_{0.5}As$ quantum dot grown using pulse jet ALE by supplying trimethylindium-dimethylethylamine adduct, trimethylgallium and arsine in an alternating fashion [89]. Compared to the Stranski-Krastanov mode MBE standard, the ALE quantum dot was more uniform in size and purer in composition, a claim supported by its single ground state emission peak under 647.1 nm Kr⁺ excitation and its narrow 30 meV full width at half-maximum from the photoluminescence spectrum [89]. In addition, the lifetime of ALE quantum dots had the ideal temperature independent lifetime up to 300 K [89]. The superior performance of ALE quantum dot was attributed to its ambiguous growth boundary and low growth rate, which facilitated the outward diffusion of defects [89].

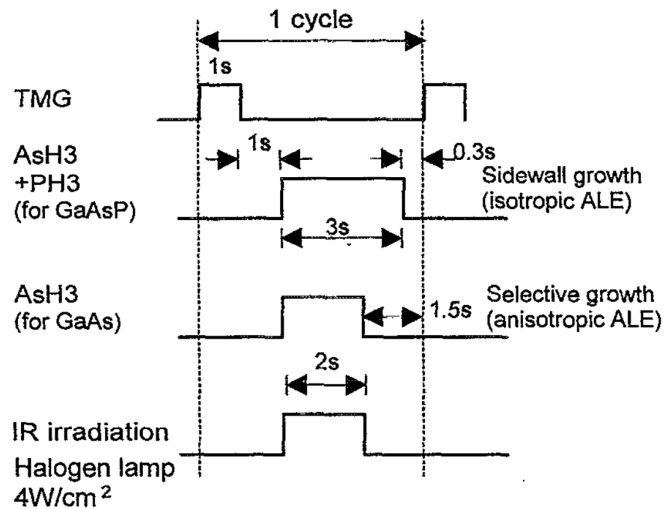


Figure 9. Growth sequence of GaAs_{0.8}P_{0.2} nanowires via ALE [85]

With the ability to tailor film composition on an atomic layer-by-layer basis, ALE enables the introduction of different periodicities within a single structure, a superlattice. Crystals with superlattices

that are not available in nature are now synthetically attainable along with their novel properties. Ferroelectricity is one example. Crystals may be roughly divided in 32 classes based on symmetry, 10 of which are pyroelectric, meaning that the materials have a spontaneous dielectric polarization [90]. Ferroelectric crystals are a subset of pyroelectrics in the sense that its polarization can be reversed by an applied electric field [90]. For its high permittivity and dielectric hysteresis properties, ferroelectrics have found applications in information storage, capacitors and amplifiers [90]. Tsurumi et al. fabricated ferroelectric superlattices of $[(\text{SrZrO}_3)_{10}/(\text{SrTiO}_3)_{10}]_4$ with the paraelectric SrZrO_3 and SrTiO_3 , evident from its clear Q-V hysteresis curve [91]. Superconductivity is another example with a wide range of applications, ranging from ultra-fast digital circuits to magnetic resonance imaging and it holds an irreplaceable role in the Large Hadron Collider of CERN [92][93][94]. The bottom line is that ALE enables researchers to construct superlattice structures with alternating layers of perovskites. To illustrate the fabrication process, for instance, Tsurumi et al. demonstrated $[(\text{BaTiO}_3)_5/(\text{SrTiO}_3)_5]_x$ oxide superlattice by MBE with RHEED where Ba and Sr were evaporated from K cells and Ti was evaporated from an EB-gun [95]. BaO , SrO and TiO_2 were oxidized by an electron cyclotron resonance plasma source. The chemical composition and crystallography of thin films were analyzed by inductively coupled plasma atomic emission spectrometry and X-ray diffractometer respectively [95]. Other common pnictogen and chalcogen superlattices have also been successfully grown, including $[(\text{CdSe})_{1-4}/(\text{ZnSe})_{10}]_{1-30}$, $[(\text{InAs})_1/(\text{GaAs})_5]_x$ and $[\text{CdTe}/\text{MnTe}]_x$ [96][97][98].

6.0 Summary

ALE has brought forth the capability of manipulating materials with atomic control. This has provided researchers a powerful tool to test out theories experimentally and realize engineering ideas that were previously unattainable. This literature review began with a brief history of ALE to illustrate how fundamentally different the process is from conventional techniques, such as evaporation, sputtering etc., from its first conception by Tuomo Suntola in 1974 [1]. For the more theoretically minded, the report dived deeper into the one-monolayer-per-cycle process with an introduction to the three epitaxial growth modes: FM, SK and VW. The review then moved on to cover different types of epitaxy processes, including SPE, LPE, VPE divided into OMVPE and MBE, and lastly ECALE. The final section of this paper discussed the many fields where ALE has been applied in and a special emphasis was given to the MBE technique for its success in growing nanostructures.

Glossary

ALE: atomic layer epitaxy
BCF: Burton, Cabrera & Franks
ECALE: electrochemical atomic layer epitaxy
EDP: electroluminescent display panels
EDTA: ethylenediaminetetraacetic acid
FM: Frank van der Merwe
FK: Frenkel-Kontorova
HPM: hydrogen peroxide / water mixture
LPE: liquid phase epitaxy
MBE: molecular beam epitaxy
MOTF: metal organic thin film
OMVPE: organometallic vapor phase epitaxy
RHEED: reflection high-energy electron diffraction
SK: Stranski-Krastanov
SPE: solid phase epitaxy
TMAH: tetramethylammonium hydroxide
UPD: under potential deposition
VPE: vapor phase epitaxy
VW: Volmer-Weber
XRD: X-ray diffraction

References

- [1] R. L. Puurunen, “A Short History of Atomic Layer Deposition: Tuomo Suntola’s Atomic Layer Epitaxy,” *Chem. Vap. Depos.*, vol. 20, no. 10–11–12, pp. 332–344, Dec. 2014.
- [2] T. Suntola, “Atomic layer epitaxy,” *Thin Solid Films*, vol. 216, no. 1, pp. 84–89, Aug. 1992.
- [3] M. Ritala and M. Leskelä, “Atomic Layer Epitaxy - A Valuable Tool For Nanotechnology?,” *Nanotechnology*, vol. 10, pp. 223–230, Mar. 1999.
- [4] A. Zangwill, “Fundamental Issues in Heteroepitaxy—A Department of Energy, Council on Materials Science Panel Report,” *J. Mater. Res.*, vol. 5, no. 4, pp. 852–894, 1990.
- [5] G. Rosenfeld *et al.*, “New concepts for controlled homoepitaxy,” *Appl. Phys. A Mater. Sci. Process.*, vol. 61, no. 5, pp. 455–466, Nov. 1995.
- [6] M. A. Herman, “Atomic layer epitaxy-12 years later,” *Vacuum*, vol. 42, no. 1–2, pp. 61–66, Jan. 1991.
- [7] T. Suntola, “Atomic layer epitaxy,” *Materials Science Reports*, vol. 4, no. 5. Elsevier, pp. 261–312, 01-Jan-1989.
- [8] H. S. Park, J. S. Min, J. W. Lim, and S. W. Kang, “Theoretical evaluation of film growth rate during atomic layer epitaxy,” *Appl. Surf. Sci.*, vol. 158, no. 1, pp. 81–91, May 2000.
- [9] K. A. Lozovoy, A. G. Korotaev, A. P. Kokhanenko, V. V. Dirkó, and A. V. Voitsekhovskii, “Kinetics of epitaxial formation of nanostructures by Frank–van der Merwe, Volmer–Weber and Stranski–Krastanow growth modes,” *Surf. Coatings Technol.*, vol. 384, p. 125289, Feb. 2020.
- [10] C. Ratsch and A. Zangwill, “Equilibrium theory of the Stranski-Krastanov epitaxial morphology,” *Surf. Sci.*, vol. 293, no. 1–2, pp. 123–131, Aug. 1993.
- [11] P. H. Fuoss, D. W. Kisker, G. Renaud, K. L. Tokuda, S. Brennan, and J. L. Kahn, “Atomic nature of organometallic-vapor-phase-epitaxial growth,” *Phys. Rev. Lett.*, vol. 63, no. 21, pp. 2389–2392, Nov. 1989.
- [12] F. Briones, D. Golmayo, L. Gonzalez, and J. L. de Miguel, “Surface stoichiometry and morphology of mbe grown (001)gaas through the analysis of rheed oscillations,” *Jpn. J. Appl. Phys.*, vol. 24, no. 6 A, pp. L478–L480, 1985.
- [13] S. A. Campbell and S. A. Campbell, *Fabrication engineering at the micro and nanoscale*. Oxford University Press, 2008.
- [14] B. A. Joyce, “Molecular beam epitaxy,” *Reports Prog. Phys.*, vol. 48, no. 12, p. 1637, 1985.
- [15] Werner Kern, “The Evolution of Silicon Wafer Cleaning Technology,” *Proc. - Electrochem. Soc.*, vol. 90, no. 9, pp. 3–19, 1990.
- [16] T. M. Pan, T. F. Lei, T. S. Chao, M. C. Liaw, F. H. Ko, and C. P. Lu, “One-Step Cleaning Solution to Replace the Conventional RCA Two-Step Cleaning Recipe for Pregate Oxide Cleaning,” *J. Electrochem. Soc.*, vol. 148, no. 6, p. G315, 2001.
- [17] K. Ryoo, B. Kang, and O. Sumita, “Electrolyzed water as an alternative for environmentally benign semiconductor cleaning,” *J. Mater. Res.*, vol. 17, no. 6, pp. 1298–1304, 2002.
- [18] B. C. Johnson, J. C. McCallum, and M. J. Aziz, “Solid-Phase Epitaxy,” in *Handbook of Crystal Growth: Thin Films and Epitaxy: Second Edition*, vol. 3, Elsevier Inc., 2015, pp. 317–363.
- [19] T. Motooka, K. Nishihira, S. Munetoh, K. Moriguchi, and A. Shintani, “Molecular-dynamics simulations of solid-phase epitaxy of Si: Growth mechanisms,” *Phys. Rev. B - Condens. Matter Mater. Phys.*, vol. 61, no. 12, pp. 8537–8540, Mar. 2000.
- [20] M. Posselt and A. Gabriel, “Atomistic simulation of amorphous germanium and its solid phase epitaxial recrystallization,” *Phys. Rev. B - Condens. Matter Mater. Phys.*, vol. 80, no. 4, p. 045202, Aug. 2009.
- [21] S. S. Lau, Z. L. Liau, and M. A. Nicolet, “Solid phase epitaxy in silicide-forming systems,” *Thin Solid Films*, vol. 47, no. 3, pp. 313–322, Dec. 1977.

- [22] H. Von Känel *et al.*, “Epitaxy of metal silicides,” *Thin Solid Films*, vol. 184, no. 1–2, pp. 295–308, Jan. 1990.
- [23] S. L. Zhang and M. Östling, “Metal silicides in CMOS technology: Past, present, and future trends,” *Critical Reviews in Solid State and Materials Sciences*, vol. 28, no. 1. CRC Press LLC, 2003.
- [24] S. Toyoda, T. Shinohara, H. Kumigashira, M. Oshima, and Y. Kato, “Significant increase in conduction band discontinuity due to solid phase epitaxy of Al₂O₃ gate insulator films on GaN semiconductor,” *Appl. Phys. Lett.*, vol. 101, no. 23, p. 231607, Dec. 2012.
- [25] T. Maeda *et al.*, “Ultrathin GeSn p-channel MOSFETs grown directly on Si(111) substrate using solid phase epitaxy,” in *Japanese Journal of Applied Physics*, 2015, vol. 54, no. 4, p. 04DA07.
- [26] B. Liu and R. A. Fischer, “Liquid-phase epitaxy of metal organic framework thin films,” *Science China Chemistry*, vol. 54, no. 12. pp. 1851–1866, Dec-2011.
- [27] R. A. Fischer and C. Wöll, “Layer-by-Layer Liquid-Phase Epitaxy of Crystalline Coordination Polymers at Surfaces,” *Angew. Chemie Int. Ed.*, vol. 48, no. 34, pp. 6205–6208, May 2009.
- [28] M. L. Ohnsorg, C. K. Beaudoin, and M. E. Anderson, “Fundamentals of MOF Thin Film Growth via Liquid-Phase Epitaxy: Investigating the Initiation of Deposition and the Influence of Temperature,” *Langmuir*, vol. 31, no. 22, pp. 6114–6121, Jun. 2015.
- [29] J. Liu *et al.*, “Deposition of metal-organic frameworks by liquid-phase epitaxy: The influence of substrate functional group density on film orientation,” *Materials (Basel)*., vol. 5, no. 9, pp. 1581–1592, 2012.
- [30] E. Biemmi, C. Scherb, and T. Bein, “Oriented growth of the metal organic framework Cu₃(BTC)₂(H₂O)₃·xH₂O tunable with functionalized self-assembled monolayers,” *J. Am. Chem. Soc.*, vol. 129, no. 26, pp. 8054–8055, Jul. 2007.
- [31] E. P. Valadez Sánchez, H. Gliemann, K. Haas-Santo, C. Wöll, and R. Dittmeyer, “ZIF-8 SURMOF Membranes Synthesized by Au-Assisted Liquid Phase Epitaxy for Application in Gas Separation,” *Chemie Ing. Tech.*, vol. 88, no. 11, pp. 1798–1805, Nov. 2016.
- [32] Y. Zhang *et al.*, “Substrate Independent Liquid Phase Epitaxy of HKUST-1 as Anticoagulant and Antimicrobial Coating,” *Adv. Mater. Interfaces*, vol. 7, no. 12, p. 1902011, Jun. 2020.
- [33] Z. G. Gu, Z. Chen, W. Q. Fu, F. Wang, and J. Zhang, “Liquid-Phase Epitaxy Effective Encapsulation of Lanthanide Coordination Compounds into MOF Film with Homogeneous and Tunable White-Light Emission,” *ACS Appl. Mater. Interfaces*, vol. 7, no. 51, pp. 28585–28590, Dec. 2015.
- [34] J. L. Zhuang, D. Ar, X. J. Yu, J. X. Liu, and A. Terfort, “Patterned deposition of metal-organic frameworks onto plastic, paper, and textile substrates by inkjet printing of a precursor solution,” *Adv. Mater.*, vol. 25, no. 33, pp. 4631–4635, Sep. 2013.
- [35] J. L. Zhuang, A. Terfort, and C. Wöll, “Formation of oriented and patterned films of metal-organic frameworks by liquid phase epitaxy: A review,” *Coordination Chemistry Reviews*, vol. 307. Elsevier B.V., pp. 391–424, 15-Jan-2016.
- [36] S. A. Campbell, “Critical review of the epitaxial growth of semiconductors by rapid thermal chemical vapor deposition,” *Mater. Sci. Eng. R Reports*, vol. 20, no. 1, pp. 1–36, Jun. 1997.
- [37] Baliga B, *Epitaxial Silicon Technology - 1st Edition*. Academic Press, 1986.
- [38] Y. Song, S. Dhar, L. C. Feldman, G. Chung, and J. R. Williams, “Modified Deal Grove model for the thermal oxidation of silicon carbide,” *J. Appl. Phys.*, vol. 95, no. 9, pp. 4953–4957, May 2004.
- [39] G. Stringfellow, *Organometallic Vapor-Phase Epitaxy*, 2nd editio. Academic Press, 1999.
- [40] C. A. Larsen, N. I. Buchan, and G. B. Stringfellow, “Reaction mechanisms in the organometallic vapor phase epitaxial growth of GaAs,” *Appl. Phys. Lett.*, vol. 52, no. 6, pp. 480–482, Feb. 1988.
- [41] K. Mukai, N. Ohtsuka, and M. Sugawara, “High photoluminescence efficiency of InGaAs/GaAs quantum dots self-formed by atomic layer epitaxy technique,” *Appl. Phys. Lett.*, vol. 70, no. 18,

- pp. 2416–2418, May 1997.
- [42] V. Lujala, J. Skarp, M. Tammenmaa, and T. Suntola, “Atomic layer epitaxy growth of doped zinc oxide thin films from organometals,” *Appl. Surf. Sci.*, vol. 82–83, no. C, pp. 34–40, Dec. 1994.
- [43] O. H. Nam, M. D. Bremser, T. S. Zheleva, and R. F. Davis, “Lateral epitaxy of low defect density GaN layers via organometallic vapor phase epitaxy,” *Appl. Phys. Lett.*, vol. 71, no. 18, pp. 2638–2640, Nov. 1997.
- [44] G. A. Rizzi, A. Magrin, and G. Granozzi, “Preparation of epitaxial ultrathin RuO₂-TiO₂(110) films by decomposition of Ru₃(CO)₁₂,” *Surf. Sci.*, vol. 443, no. 3, pp. 277–286, Dec. 1999.
- [45] G. B. Stringfellow, “Fundamental aspects of organometallic vapor phase epitaxy,” *Materials Science and Engineering B: Solid-State Materials for Advanced Technology*, vol. 87, no. 2. Elsevier, pp. 97–116, 15-Nov-2001.
- [46] J. R. Arthur, “Molecular beam epitaxy,” *Surf. Sci.*, vol. 500, no. 1–3, pp. 189–217, Mar. 2002.
- [47] M. A. Herman and H. Sitter, *Molecular Beam Epitaxy*, vol. 7. Berlin, Heidelberg: Springer Berlin Heidelberg, 1996.
- [48] W. Kern, *Thin Film Processes II*, 1st editio. Academic Press, 2012.
- [49] R. Ghez and S. S. Iyer, “Kinetics of fast steps on crystal surfaces and its application to the molecular beam epitaxy of silicon,” *IBM J. Res. Dev.*, vol. 32, no. 6, pp. 804–818, 1988.
- [50] K. Ploog, “Molecular Beam Epitaxy of III–V Compounds,” Springer, Berlin, Heidelberg, 1980, pp. 73–162.
- [51] M. D. La Mata *et al.*, “A review of MBE grown 0D, 1D and 2D quantum structures in a nanowire,” *Journal of Materials Chemistry C*, vol. 1, no. 28. Royal Society of Chemistry, pp. 4300–4312, 28-Jul-2013.
- [52] J. Redepenning, “Electroanalytical Chemistry: A Series of Advances, Volume 22 Edited by Allen J. Bard (University of Texas at Austin) and Israel Rubinstein (Weizmann Institute of Science). Marcel Dekker, Inc.: New York, Basel. 2003. xx + 310 pp. \$199.00. ISBN: 0-8247-4,” *J. Am. Chem. Soc.*, vol. 126, no. 30, pp. 9465–9466, Aug. 2004.
- [53] S. Szabó, “Underpotential deposition of metals on foreign metal substrates,” *Int. Rev. Phys. Chem.*, vol. 10, no. 2, pp. 207–248, 1991.
- [54] B. W. Gregory and J. L. Stickney, “Electrochemical atomic layer epitaxy (ECALE),” *J. Electroanal. Chem.*, vol. 300, no. 1–2, pp. 543–561, Feb. 1991.
- [55] L. P. Colletti, “Formation of Thin Films of CdTe, CdSe, and CdS by Electrochemical Atomic Layer Epitaxy,” *J. Electrochem. Soc.*, vol. 145, no. 5, p. 1442, 1998.
- [56] B. H. Flowers, T. L. Wade, J. W. Garvey, M. Lay, U. Happek, and J. L. Stickney, “Atomic layer epitaxy of CdTe using an automated electrochemical thin-layer flow deposition reactor,” *J. Electroanal. Chem.*, vol. 524–525, pp. 273–285, May 2002.
- [57] R. Vaidyanathan, J. L. Stickney, and U. Happek, “Quantum confinement in PbSe thin films electrodeposited by electrochemical atomic layer epitaxy (EC-ALE),” in *Electrochimica Acta*, 2004, vol. 49, no. 8, pp. 1321–1326.
- [58] I. Villegas, “Preliminary Studies of GaAs Deposition on Au(100), (110), and (111) Surfaces by Electrochemical Atomic Layer Epitaxy,” *J. Electrochem. Soc.*, vol. 139, no. 3, p. 686, 1992.
- [59] S. Feng *et al.*, “CdS quantum dots sensitized TiO₂ nanorod-array-film photoelectrode on FTO substrate by electrochemical atomic layer epitaxy method,” *Electrochim. Acta*, vol. 83, pp. 321–326, Nov. 2012.
- [60] J. Zhang *et al.*, “Fabrication of CdTe Quantum Dots Sensitized TiO₂ Nanorod-Array-Film Photoanodes via the Route of Electrochemical Atomic Layer Deposition ,” *J. Electrochem. Soc.*, vol. 161, no. 1, pp. D55–D58, Nov. 2014.
- [61] S. Feng *et al.*, “Epitaxial growth of successive CdSe ultrathin films and quantum dot layers on TiO₂ nanorod arrays for photo-electrochemical cells,” *RSC Adv.*, vol. 4, no. 24, pp. 12154–

- 12159, Feb. 2014.
- [62] S. Zou and M. J. Weaver, "Surface-enhanced Raman spectroscopy of cadmium sulfide/cadmium selenide superlattices formed on gold by electrochemical atomic-layer epitaxy," *Chem. Phys. Lett.*, vol. 312, no. 2–4, pp. 101–107, Oct. 1999.
- [63] W. Zhu, J. Y. Yang, D. X. Zhou, C. J. Xiao, and X. K. Duan, "Electrochemical aspects and structure characterization of VA-VIA compound semiconductor Bi₂Te₃/Sb₂Te₃ superlattice thin films via electrochemical atomic layer epitaxy," *Langmuir*, vol. 24, no. 11, pp. 5919–5924, Jun. 2008.
- [64] R. Vaidyanathan, S. M. Cox, U. Happek, D. Banga, M. K. Mathe, and J. L. Stickney, "Preliminary studies in the electrodeposition of PbSe/PbTe superlattice thin films via electrochemical atomic layer deposition (ALD)," *Langmuir*, vol. 22, no. 25, pp. 10590–10595, Dec. 2006.
- [65] N. Goel, P. Majhi, C. O. Chui, W. Tsai, D. Choi, and J. S. Harris, "InGaAs metal-oxide-semiconductor capacitors with HfO₂ gate dielectric grown by atomic-layer deposition," *Appl. Phys. Lett.*, vol. 89, no. 16, p. 163517, Oct. 2006.
- [66] A. D. Koehler *et al.*, "Atomic layer epitaxy AlN for enhanced AlGaN/GaN HEMT passivation," *IEEE Electron Device Lett.*, vol. 34, no. 9, pp. 1115–1117, 2013.
- [67] Y. M. Lin *et al.*, "100-GHz transistors from wafer-scale epitaxial graphene," *Science*, vol. 327, no. 5966. American Association for the Advancement of Science, p. 662, 05-Feb-2010.
- [68] J. Park *et al.*, "Epitaxial Graphene Growth by Carbon Molecular Beam Epitaxy (CMBE)," *Adv. Mater.*, vol. 22, no. 37, pp. 4140–4145, Aug. 2010.
- [69] E. Moreau, F. J. Ferrer, D. Vignaud, S. Godey, and X. Wallart, "Graphene growth by molecular beam epitaxy using a solid carbon source," *Phys. status solidi*, vol. 207, no. 2, pp. 300–303, Feb. 2010.
- [70] E. Moreau *et al.*, "Graphene growth by molecular beam epitaxy on the carbon-face of SiC," *Appl. Phys. Lett.*, vol. 97, no. 24, p. 241907, Dec. 2010.
- [71] B. von Roedern, "How do Buffer Layers Affect Solar Cell Performance and Solar Cell Stability?," *MRS Proc.*, vol. 668, p. H6.9, Mar. 2001.
- [72] E. B. Yousfi, T. Asikainen, V. Pietu, P. Cowache, M. Powalla, and D. Lincot, "Cadmium-free buffer layers deposited by atomic layer epitaxy for copper indium diselenide solar cells," *Thin Solid Films*, vol. 361, pp. 183–186, Feb. 2000.
- [73] W. M. M. Kessels, B. Hoex, and M. C. M. Van De Sanden, "Atomic layer deposition: Prospects for solar cell manufacturing," in *Conference Record of the IEEE Photovoltaic Specialists Conference*, 2008.
- [74] M. Asif Khan *et al.*, "Stripe geometry ultraviolet light emitting diodes at 305 nanometers using quaternary AlInGaN multiple quantum wells," *Japanese J. Appl. Physics, Part 2 Lett.*, vol. 40, no. 12 A, p. 1308, Dec. 2001.
- [75] J. P. Zhang *et al.*, "Algan multiple-quantum-well-based, deep ultraviolet light-emitting diodes with significantly reduced long-wave emission," *Appl. Phys. Lett.*, vol. 83, no. 17, pp. 3456–3458, Oct. 2003.
- [76] V. Adivarahan *et al.*, "Ultraviolet light-emitting diodes at 340 nm using quaternary AlInGaN multiple quantum wells," *Applied Physics Letters*, vol. 79, no. 25. American Institute of PhysicsAIP, pp. 4240–4242, 17-Dec-2001.
- [77] K. Kukli, "Properties of Ta_[sub 2]O_[sub 5]-Based Dielectric Nanolaminates Deposited by Atomic Layer Epitaxy," *J. Electrochem. Soc.*, vol. 144, no. 1, p. 300, 1997.
- [78] D. Riihelä, M. Ritala, R. Matero, and M. Leskelä, "Introducing atomic layer epitaxy for the deposition of optical thin films," *Thin Solid Films*, vol. 289, no. 1–2, pp. 250–255, Nov. 1996.
- [79] J. S. King, D. Heineman, E. Graugnard, and C. J. Summers, "Atomic layer deposition in porous structures: 3D photonic crystals," in *Applied Surface Science*, 2005, vol. 244, no. 1–4, pp. 511–

- [80] R. J. Narayan, N. A. Monteiro-Riviere, R. L. Brigmon, M. J. Pellin, and J. W. Elam, "Atomic layer deposition of TiO₂ thin films on nanoporous alumina templates: Medical applications," *JOM*, vol. 61, no. 6. Springer, pp. 12–16, 10-Jun-2009.
- [81] E. Kapon, S. Simhony, R. Bhat, and D. M. Hwang, "Single quantum wire semiconductor lasers," *Appl. Phys. Lett.*, vol. 55, no. 26, pp. 2715–2717, Dec. 1989.
- [82] O. E. Semonin *et al.*, "Peak external photocurrent quantum efficiency exceeding 100% via MEG in a quantum dot solar cell," *Science (80-)*, vol. 334, no. 6062, pp. 1530–1533, Dec. 2011.
- [83] N. Usami, T. Mine, S. Fukatsu, and Y. Shiraki, "Realization of crescent-shaped SiGe quantum wire structures on a V-groove patterned Si substrate by gas-source Si molecular beam epitaxy," *Appl. Phys. Lett.*, vol. 63, no. 20, pp. 2789–2791, Nov. 1993.
- [84] J. Wang, B. J. Robinson, D. A. Thompson, and J. G. Simmons, "InGaAs/InP quantum wires grown by gas source molecular beam epitaxy onto V-grooved InP substrates with (111)A facet sidewalls," *Appl. Phys. Lett.*, vol. 67, no. 16, p. 2358, Oct. 1995.
- [85] H. Isshiki, Y. Aoyagi, T. Sugano, S. Iwai, and T. Meguro, "Characterization of GaAs/GaAsP quantum wire structures fabricated by atomic layer epitaxy," *J. Appl. Phys.*, vol. 78, no. 12, pp. 7277–7281, Dec. 1995.
- [86] I. V. Kudryashov, V. P. Evtikhev, V. E. Tokranov, E. Y. Kotel'nikov, A. K. Kryganovskii, and A. N. Titkov, "Effect of GaAs(0 0 1) surface misorientation on the emission from MBE grown InAs quantum dots," *J. Cryst. Growth*, vol. 201, pp. 1158–1160, May 1999.
- [87] S. Fukatsu, H. Sunamura, Y. Shiraki, and S. Komiyama, "Suppression of phonon replica in the radiative recombination of an MBE-grown type-II Ge/Si quantum dot," *Thin Solid Films*, vol. 321, no. 1–2, pp. 65–69, May 1998.
- [88] A. Karim, G. V. Hansson, W. X. Ni, P. O. Holtz, M. Larsson, and H. A. Atwater, "Photoluminescence studies of Sn quantum dots in Si grown by MBE," in *Optical Materials*, 2005, vol. 27, no. 5, pp. 836–840.
- [89] K. Mukai, N. Ohtsuka, and M. Sugawara, "High photoluminescence efficiency of InGaAs/GaAs quantum dots self-formed by atomic layer epitaxy technique," *Appl. Phys. Lett.*, vol. 70, no. 18, pp. 2416–2418, May 1997.
- [90] R. C. Kell, "Modern applications of ferroelectricity," IOP Publishing, May 1963.
- [91] T. Tsurumi *et al.*, "Artificial ferroelectricity in perovskite superlattices," *Appl. Phys. Lett.*, vol. 85, no. 21, pp. 5016–5018, Nov. 2004.
- [92] A. H. Silver, "Superconductivity in electronics," *IEEE Trans. Appl. Supercond.*, vol. 7, no. 2 PART 1, pp. 69–79, 1997.
- [93] "Magnetic Resonance Imaging, a success story for superconductivity | Europhysics News." [Online]. Available: <https://www.europhysicsnews.org/articles/epn/abs/2012/04/epn2012434p26/epn2012434p26.html>. [Accessed: 24-Jul-2020].
- [94] L. Rossi, "EUROPEAN ORGANIZATION FOR NUCLEAR RESEARCH CERN-ACCELERATORS AND TECHNOLOGY SECTOR SUPERCONDUCTIVITY: ITS ROLE, ITS SUCCESS AND ITS SETBACK IN THE LARGE HADRON COLLIDER (LHC) OF CERN," Jan. 2010.
- [95] T. Tsurumi, T. Suzuki, M. Yamane, and M. Daimon, "Fabrication of barium titanate/strontium titanate artificial superlattice by atomic layer epitaxy," *Jpn. J. Appl. Phys.*, vol. 33, no. 9 S, pp. 5192–5195, 1994.
- [96] T. Matsumoto, T. Iwashita, K. Sasamoto, and T. Kato, "Atomic layer epitaxy of CdSe/ZnSe short period superlattices," *J. Cryst. Growth*, vol. 138, no. 1–4, pp. 63–67, Apr. 1994.
- [97] K. Mori, S. Sugou, Y. Kato, and A. Usui, "Growth of InAs and (InAs)₁(GaAs)₅ superlattice by atomic layer epitaxy using dimethylindium chloride," *Appl. Phys. Lett.*, vol. 60, no. 14, pp.

1717–1719, Apr. 1992.

- [98] J. M. Hartmann, G. Feuillet, M. Charleux, and H. Mariette, “Atomic layer epitaxy of CdTe and MnTe,” *J. Appl. Phys.*, vol. 79, no. 6, pp. 3035–3041, Mar. 1996.